Resolving the Rise and Fall of Star Formation in Galaxies
Proceedings IAU Symposium No. 373, 2023
T. Wong & W.-T. Kim, eds.
doi:10.1017/S1743921322003763

Gas-Star Formation Cycle in Nearby Galaxies

Hsi-An Pan[1], Eva Schinnerer[2], Annie Hughes[3], Adam Leroy[4], Brent Groves[5] and The PHANGS Team

[1]Department of Physics, Tamkang University, No.151, Yingzhuan Road, Tamsui District, New Taipei City 251301, Taiwan
email: hapan@gms.tku.edu.tw

[2]Max-Planck-Institut für Astronomie, Königstuhl 17, D-69117 Heidelberg, Germany

[3]CNRS, IRAP, Av. du Colonel Roche BP 44346, F-31028 Toulouse cedex 4, France

[4]Department of Astronomy, The Ohio State University, 140 West 18th Ave, Columbus, OH 43210, USA

[5]International Centre for Radio Astronomy Research, The University of Western Australia, Crawley, WA 6009, Australia

Abstract. Star formation, from cold giant molecular clouds to diverse population of stars, is a complex process involving a wide variety of physical processes. In this work, we constrain the link between the gas-star formation cycle and several secular and environmental probe of galaxies. Specifically, we quantify the spatial correlation between molecular gas and star-forming regions for 49 nearby galaxies using the ALMA and narrowband-Hα imaging from the PHANGS survey. At the resolution (150 pc) at which the individual molecular clouds and star-forming regions can be identified, we find that molecular clouds and star-forming regions do not necessarily coexist. The decoupled molecular clouds and star-forming regions are a signature of evolutionary cycling and feedback of the star formation process. Therefore, the impact of galactic-scale conditions and environments must be considered for a complete understanding of how stars form in galaxies and how this process influences the evolution of the host galaxies.

Keywords. ISM: clouds, stars: formation, galaxies: evolution

1. Introduction

Star formation is a complex process that requires tracing cloud formation, fragmentation, and evolution within the local parsec to 100 pc scale and galactic to large-scale environment at kilo-parsec to mega-parsec scales. Schmidt (1959) observed a tight correlation between the star formation rate (SFR) and the volume density of gas in the Milky Way. Later on, Kennicutt (1998) found that the galaxy-integrated SFR surface density (Σ_{SFR}) and gas surface density (Σ_{gas}) also follow a similar power-law relation for nearby galaxies. The relation is now known as the Schmidt-Kennicutt relation. Recently the improvement in spatial resolution brought by instruments such as GALEX, VLA, IRAM 30-m telescope, and BIMA have allowed the Schmidt-Kennicutt relation to be probed on sub-kpc scales (e.g., Bigiel et al. 2008). They show that, on sub-kpc scales, Σ_{SFR} is directly related to molecular gas (Σ_{H_2}) with a power-law index around unity, while the relationship between Σ_{SFR} and total gas (Σ_{gas}) is rather loose. The linear relationship between Σ_{SFR} and Σ_{H_2} implies a roughly constant H_2 consumption time; namely, star formation proceeds in a uniform way in molecular gas in nearby spiral galaxies.

However, cloud-scale ($\sim$ 100 pc) observations in the Local Group and a few nearby star-forming galaxies suggest a more complex picture. The scatter in the Schmidt-Kennicutt relation increase with improving spatial resolution (e.g., Onodera et al. 2010, Kreckel et al. 2018). This is because when the resolution approaches the scale of individual giant molecular clouds (GMCs) and star-forming regions (e.g., HII regions), tracers of massive stars and cold molecular gas become spatially distinct. On the small scale, the scatter in the Schmidt-Kennicutt relation has been interpreted as a results of the evolution of GMCs and the impact of destructive stellar feedback on the structure of interstellar medium (ISM) (e.g., photoionization, stellar winds, and supernova explosions). On the other hand, on the large scale, various environmental mechanisms, such as galactic shear, noncircular motions, gas flows along and through stellar dynamical structures (e.g., bars and spiral arms), and accretion flows also play a role to determine when and which pockets of the GMCs collapse (e.g., Jeffreson et al. 2020), and therefore the relative distribution of GMCs and star-forming regions.

In this work (Pan et al. 2022), we develop a simple and robust method that quantifies the relative spatial distributions of molecular gas and recent star formation, as well as the spatial scale dependence of the relative distributions. The method considers the presence or absence of molecular gas traced by CO emission and star formation traced by Hα emission in a given region (i.e., sight-line or pixel) at a given observed resolution. The method, in principle, is able to provide more information on the gas-to-star formation cycle than the Schmidt-Kennicutt relation as the Schmidt-Kennicutt relation, by definition, only consider the regions where both molecular gas and recent star formation coexist, while at cloud-scale ($\sim$ 100 pc) resolution, such region only accounts for a small fraction of regions with emission.

2. Data and Analysis

The data of this work is taken from the PHANGS (Physics at High Angular resolution in Nearby GalaxieS)† survey. PHANGS is a multi-wavelength survey to observe the tracers of the full star formation process (from gas to star clusters) in a diverse sample of nearby galaxies. The typical spatial resolution achieved with the multi-wavelength observations is about 100 pc. The galaxies are lying on or near the star-forming main sequence. More details on the survey design and scientific motivation are presented in Leroy et al. (2021). In this work, we focus on the molecular gas and ionized (Hα) gas observed by the PHANGS-ALMA and PHANGS-Hα (narrowband) surveys, respectively. 49 galaxies are used in this work.

Our analysis uses Hα as a tracer for the location of recent high-mass star formation. A two-step unsharp masking technique is used to remove the diffuse ionized gas (DIG) from the Hα images. A step-by-step, quantitative description of the method is described in Schinnerer et al. (2019) and Pan et al. (2022). On average, about 65% of the Hα emission across the sample is removed by the DIG removal process.

The CO images are treated using a similar scheme. We clip the CO images at our best-matching resolution of 150 pc using a Σ_{H_2} threshold of 10 $M_\odot$ pc^{-2} accounting for galaxy inclination. This corresponds to a 3σ Σ_{H_2} sensitivity of our CO map with the lowest sensitivity at this spatial scale.

Finally, we measure the presence or absence of the two tracers at each resolution in an field-of-view extending to 0.6 R_{25}, which is the largest radial extent probed by our data in all galaxies, corresponding to $\sim$6.4 kpc on average. We classify each sight line (pixel) within 0.6 R_{25} in the CO and Hα images into one of four categories: *CO-only* – only CO emission is present, *Hα-only* – only Hα emission is present, *overlap* – both CO and

† www.phangs.org

https://doi.org/10.1017/S1743921322003763 Published online by Cambridge University Press

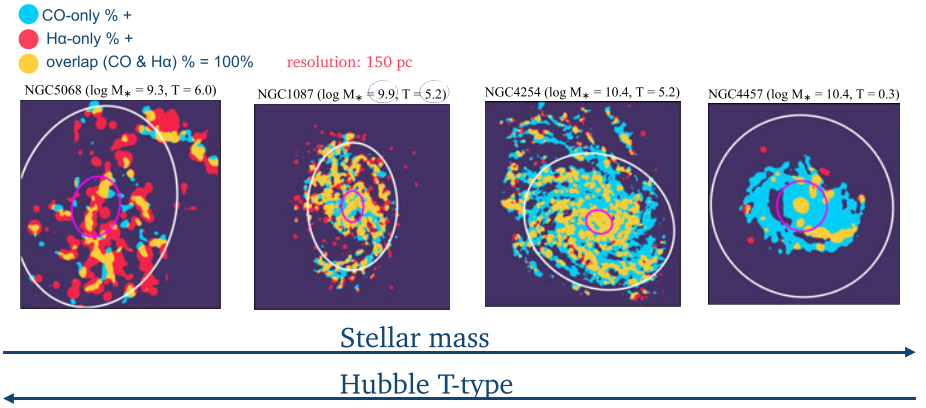

Figure 1. Examples of the spatial distribution of different sight lines. Galaxy maps show the regions of *CO-only* (blue), *Hα-only* (red), and *overlap* (yellow) sight lines at 150 pc resolution. The inner ellipses (magenta) mark the central region, defined as the central 2 kpc in deprojected diameter. The outer ellipses (white) indicate the $0.6R_{25}$ regions where we measure the global sight line fractions.

Hα emission are present, and *empty* – neither CO nor Hα emission is present. In this work, we do not consider the *empty* sight lines but measure the fraction of sight lines in *CO-only*, *Hα-only*, and *overlap* regions at each resolution.

3. Results and Discussion

3.1. *Sight-line Distribution*

Figure 1 shows the examples of the spatial distribution of different sight lines. As seen in the figure, our galaxies show diverse relative distribution of CO and Hα emission. In our sample, some galaxies, such as NGC 5068, are dominated by *Hα-only* regions, while some galaxies, e.g., NGC 4457 are dominated by *CO-only* regions.

3.2. *Sight line Fractions vs. Global Galaxy Properties*

Figure 2 shows box plots of sight line fractions as a function of stellar mass (left) and Hubble type (right). Galaxies are divided into three groups according to their stellar mass or Hubble type. The darker colors indicate increasing stellar mass or decreasing Hubble-type value. The inner horizontal belt-like symbol and line in the boxes represent the median and mean of the distribution, respectively The left panel of Figure 2 shows a tendency for more massive galaxies to have higher *CO-only* fractions. The opposite trend is exhibited by *Hα-only* fractions. The median *overlap* fractions remain at a nearly constant value, ∼30%, as a function of stellar mass. In the right panel of Figure 2, the fraction of *CO-only* sight lines deceases with Hubble type, and the fraction of *Hα-only* sight lines increases with Hubble type. The trends with Hubble type and stellar mass are consistent in the sense that late-type galaxies tend to be less massive.

Moreover, Figure 2 implies that if the CO and Hα images at 150 pc resolution are used to construct the Schimdt-Kennicutt relation as a diagnostic of star formation process, only 30% of sight lines (the *overlap* regions) would show in the relation. As a result, we might be missing important variation in gas depletion time (the slope and intercept of the Schmidt-Kennicutt relation) and change in cloud life cycle/time variations (i.e., scatter of the relation).

https://doi.org/10.1017/S1743921322003763 Published online by Cambridge University Press

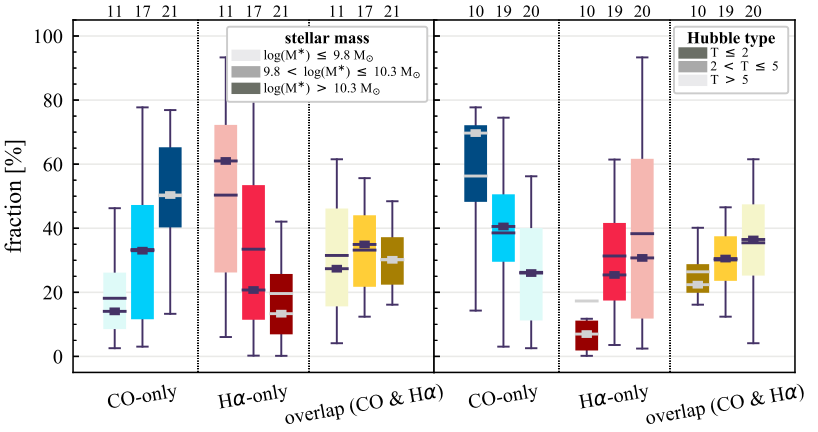

Figure 2. Global sight line fractions at 150 pc resolution as a function of stellar mass (left) and Hubble type (right). The boxes show the interquartile ranges (IQR; the Q1/25 percentile to Q3/75 percentile), and the vertical whiskers extend to Q1 - 1.5 × IQR and Q3 + 1.5 × IQR. The inner horizontal belt-like symbol and line in the boxes represent the median and mean of the distribution, respectively. The number of galaxies in each stellar mass and Hubble-type bin are shown at the top of the plots.

3.3. *Sight-line Fractions vs. Dynamical Structures*

In addition to global galaxy properties, we can also classify galaxies according to their dynamical structures, such as the presence of stellar bar and spiral arms. We classify galaxies into four groups:

- No Structure (NS): galaxies without a bar and grand-design (GD) spiral arms (e.g., galaxies with flocculent/multiple arms are in this category),
- Bar:galaxies with a bar but no GD spiral arms,
- Bar+GD: galaxies with a bar and GD spiral arms,
- GD: galaxies with GD arms but without a bar.

The corresponding box plots are shown in Figure 3.

We find a sign for galaxies with only grand-design spiral arms to show higher fraction of *CO-only* regions and lower *Hα-only* regions. Some galaxies in our sample show a pronounced offset between the different sight line types with a sequence of *CO-only* to *overlap* and to *Hα-only* when going from up- to downstream (assuming the spiral arms are trailing, e.g., NGC 4321, NGC 0628, NGC 1566, and NGC 2997). The offset of different types of sight lines is consistent with expectations for a spiral density wave. These offsets are almost exclusively found in galaxies with well-defined grand-design spiral arms and presumably lead in turn to the high *CO-only* fraction in the disk.

3.4. *Physical Interpretation of Different Types of Sight lines*

What do the three types of sight line mean physically? We find a large reservoir of molecular gas traced by CO not associated with star-forming regions in our galaxies. One of the most interesting result in this work is that the molecular gas surface density of *CO-only* regions are not necessarily low, ranging from 10 (the applied threshold) to several thousands solar mass per parsec square. These high-density *CO-only* regions could be pre-star-forming clouds, they are still undergoing gravitational collapse; or, massive stars may be already formed in part of the *CO-only* gas, but their Hα emission is obscured by dust. Some CO-only regions might be a diffuse, dynamically hot component (Pety et al. 2013) that is not prone to star formation or may be analogous to the gas in the centers of early-type (elliptical) galaxies. It is also possible that high-mass star formation is suppressed in

https://doi.org/10.1017/S1743921322003763 Published online by Cambridge University Press

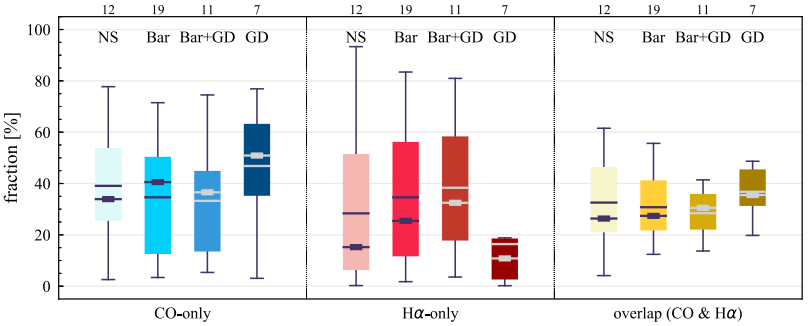

Figure 3. Sight line fractions at 150 pc resolution for galaxies without structures (bar or grand-design spiral arms; NS), galaxies with a bar but without grand-design spiral arms (Bar), galaxies with both a bar and grand-design spiral arms (Bar+GD), and galaxies with grand-design spiral arms but no bar (GD).

some *CO-only* regions, forming stars that are not massive enough to produce detectable Hα emission.

The *overlap* regions are typical star-forming regions where molecular gas and stars coexist. Finally, about one-third of sight-lines show Hα emission not associated with molecular gas. Molecular gas might be completely consumed by star formation in these regions, so star formation will halt at some point in these regions in the near future unless there is additional supply of molecular gas. It is also possible that these regions have experienced significant stellar feedback which destroys the parent molecular clouds of the star forming regions.

In conclusion, the different types of sight-lines represent different phases of star formation. Therefore, different relative distribution of CO and Hα implies different gas-to-star formation cycle in galaxies.

3.5. *Impact of Spatial Scale*

With high-resolution images, we can investigate the impact of spatial scale on the distributions of CO and Hα emission. Figure 4 shows the sight line fractions for three example galaxies as a function of spatial scale from 150 pc to 1.5 kpc. The figure shows that, no matter which type of the sight-line dominate the images at 150 pc resolution, at 1.5 kpc resolution, the *overlap* region become the dominant one. This is simply because the CO and Hα images become similar when we lower the resolution. For all sight line categories, the variations with spatial scale become less evident at > 500 pc resolution, indicating a critical resolution requirement to resolve the gas-to-star formation cycle in nearby galaxies.

4. Summary

In this work, we adopt a simple and reproducible method developed to quantify the relative spatial distributions of molecular gas and recent star formation. We classify each sight line (i.e., pixel) at each resolution according to the overlap between the tracers: *CO-only*, *Hα-only*, and *overlap* (CO and Hα). These three categories can be translated into the following star formation phases: *CO-only* – molecular gas currently not associated with star formation traced by Hα, *overlap* – star-forming molecular clouds, and *Hα-only* –regions of young massive stars. The best common resolution of our galaxies (150 pc) is sufficiently high to sample individual star-forming units and to separate different types of sight lines.

https://doi.org/10.1017/S1743921322003763 Published online by Cambridge University Press

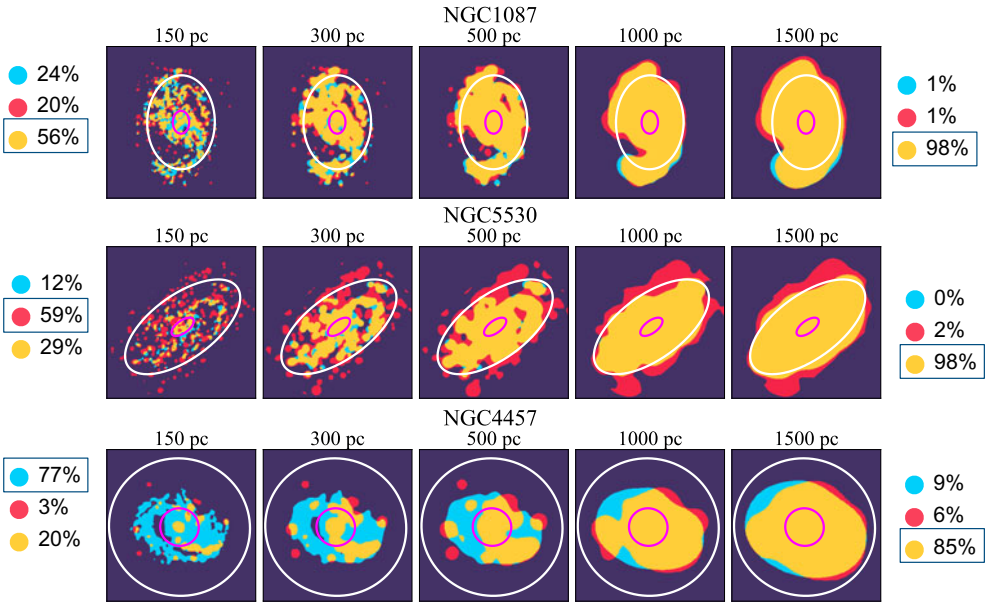

Figure 4. Sight line map as a function of spatial scale. The colors and symbols are the same as in Figure 1.

At 150 pc resolution, we find strong correlations between the sight-line fractions and global galaxy properties (stellar mass and Hubble type). In addition, galactic dynamics further contributes to organizing the spatial configuration of molecular gas and star-forming regions within galaxies. Since different types of sight lines represent different phases of star formation, the different relative amount and spatial distribution of molecular gas traced by CO and star-forming regions traced by Hα implies different gas-to-star formation cycle in nearby galaxies.

Finally the sight line fractions show a strong dependence on the spatial scale (resolution). Any relation between the sight line fractions and galaxy properties are only evident when the resolution is higher than 500 pc, suggesting the importance of cloud-scale resolution on the studies of star formation in nearby galaxies.

References

Bigiel, F., Leroy, A., Walter, F., et al. 2008, AJ, 136, 2846. doi:10.1088/0004-6256/136/6/2846
Jeffreson, S. M. R., Kruijssen, J. M. D., Keller, B. W., et al. 2020, MNRAS, 498, 385. doi:10.1093/mnras/staa2127
Kreckel, K., Faesi, C., Kruijssen, J. M. D., et al. 2018, ApJL, 863, L21. doi:10.3847/2041-8213/aad77d
Leroy, A. K., Schinnerer, E., Hughes, A., et al. 2021, ApJS, 257, 43. doi:10.3847/1538-4365/ac17f3
Onodera, S., Kuno, N., Tosaki, T., et al. 2010, ApJL, 722, L127. doi:10.1088/2041-8205/722/2/L127
Pan, H.-A., Schinnerer, E., Hughes, A., et al. 2022, ApJ, 927, 9. doi:10.3847/1538-4357/ac474f
Pety, J., Schinnerer, E., Leroy, A. K., et al. 2013, ApJ, 779, 43. doi:10.1088/0004-637X/779/1/43
Schinnerer, E., Hughes, A., Leroy, A., et al. 2019, ApJ, 887, 49. doi:10.3847/1538-4357/ab50c2
Schmidt, M. 1959, ApJ, 129, 243. doi:10.1086/146614